Multi-Port Converter Integrating Bidirectional Converters and Induction Heating Inverter for Electric Vehicles

Satoru Onodera
Graduate School of Sci. and Eng.
Ibaraki Univ.
Hitachi, Ibaraki, Japan
20nm611t@vc.ibaraki.ac.jp

Motoki Sato
Graduate School of Sci. and Eng.
Ibaraki Univ.
Hitachi, Ibaraki, Japan
19nm633t@vc.ibaraki.ac.jp

Masatoshi Uno
Graduate School of Sci. and Eng.
Ibaraki Univ.
Hitachi, Ibaraki, Japan
masatoshi.uno.ee@vc.ibaraki.ac.jp

***Abstract*—Multi-port converters (MPCs) that integrate a dual active bridge (DAB) converter and an interleaved PWM converter have been proposed to reduce the converter count in electric vehicle power systems where multiple rechargeable batteries are employed. On the other hand, EVs require external heaters, due to the lack of wasted heat from engines, resulting in increased system cost. This paper proposes a novel MPC with induction heating (IH) capability as a potential solution to reduce the cost of EV power systems. The detailed operation analysis for the proposed MPC is performed to reveal that the output power of the IH inverter can be independently regulated by phase-shift control. Experimental results of a 1-kW prototype demonstrated the proposed MPC could transmit power among batteries and regulate the IH power simultaneously.**

Keywords— DAB Converter, induction heating, interleaved PWM converter, multi-port converter

I. Introduction

In recent years, electric vehicles (EVs) have been becoming increasingly popular to reduce the emission of greenhouse gas. The development of compact, low-cost, and highly efficient EV power systems has been underway. A conventional EV power system is illustrated in Fig. 1(a). The EV power system consists of multiple batteries, including A high-voltage battery (HVB) to drive the main motor, 12-V low-voltage battery (LVB) and 48-V middle-voltage battery (MVB) for auxiliary equipment. EV power systems tend to be complex and costly because multiple bidirectional converters are needed to control each battery individually.

Multi-port converters (MPCs) integrating multiple isolated or nonisolated converters into a single unit have been proposed [1]–[11] in order to achieve the simplified system and low-cost [Fig. 1(b)]. On the other hand, EVs require heat sources, such as electric heaters or heat pumps, due to the lack of wasted heat from engines.

A conventional MPC for EV power systems is shown in Fig. 2 [1]. The conventional MPC is derived from integrating a nonisolated interleaved PWM converter [17] and an isolated dual active bridge (DAB) converter [18]. The circuit on the transformer's primary side, or a low-voltage side, consists of a two-phase interleaved bidirectional PWM converter. The interleaved PWM converter reduces current ripples and

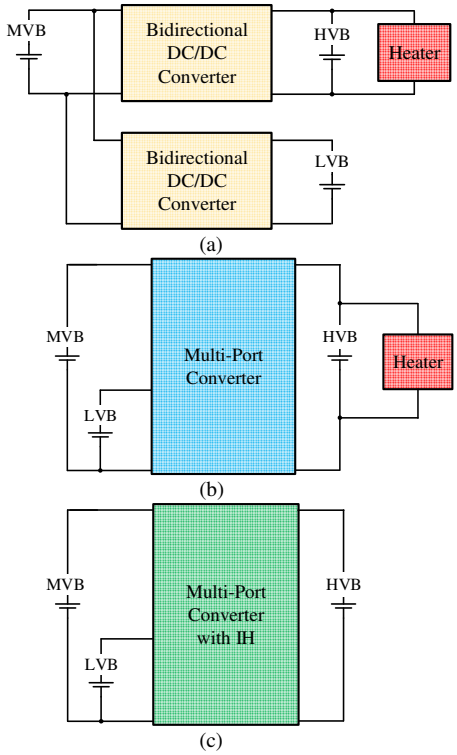

Fig. 1 Models of the EV power system (a)a conventional system (b)a conventional system with MPC (c) the proposed system

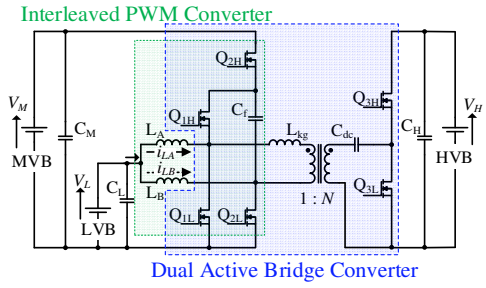

Fig. 2. The conventional MPC

enhances the current capacity of the LVB port. A flying capacitor C_f is inserted between switches Q_{2L} and Q_{2H} to achieve not only an automatic capacitive current balancing for

inductors of L_A and L_B but also a high voltage-conversion ratio between the LVB (V_L) and MVB (V_M). The secondary side, or a high-voltage side, consists of a half-bridge rectifier with a dc blocking capacitor C_{dc} to prevent dc bias current of the transformer. C_{dc} also behaves as a voltage doubler that contributes to reducing the number of secondary winding turns. Thanks to the integration of the two bidirectional converters, the conventional MPC achieves the bidirectional power flow among all three batteries and a simplified system [1]–[2]. However, the increased system cost due to the necessity of heat sources still remains as a challenge in EV power systems [Fig. 1(b)].

In general, external heaters such as positive temperature coefficient (PTC) heaters or heat pumps are employed as a heat source in EVs. PTC heaters have a quick response and high heating capacity, but their heating efficiency is relatively low in comparison with other heating techniques [22]–[23]. Heat pumps are advantageous in terms of safety, but the decreased heating capability at low ambient temperatures is a major concern [24]–[25]. Furthermore, these heaters tend to be complex and costly as they require a lot of auxiliary parts.

Meanwhile, the induction heating (IH) is one of the most widely used heating methods to heat metallic materials [12]–[16], [19], [26]–[27]. Compared to external heating methods, such as electric heaters and heat pumps, the heating efficiency of IH is high because IH heats the workpiece from inside. IH heaters, a contactless heating method, would be suitable for EVs from the viewpoints of safety and volume, contributing to cost and volume reduction of EV power systems.

This paper presents the MPC integrating an IH inverter for EVs [Fig. 1(c)]. The MPC and IH inverter are integrated with sharing semiconductor switches, and therefore, the IH heating capability can be realized with only a few additional circuit elements.

The rest of this paper is organized as follows. Section II describes the derivation and control scheme of the proposed MPC. The operational analysis and theoretical characteristic of the IH inverter will be presented in Section III. The experimental results of a 1-kW prototype will be shown to demonstrate the proposed MPC in Section IV, followed by the conclusion in Section V.

II. Proposed MPC

A. Derivation and Features

Fig. 3 shows the proposed MPC for EVs. Adding a switching leg of Q_{4L}–Q_{4H} and an LC tank to the high-voltage side of the conventional MPC derives the proposed MPC. A phase-shift (PS)-controlled full-bridge IH inverter is configured by sharing switches (Q_{3L}–Q_{3H}) that are the key elements for both the DAB converter and IH inverter.

In addition to the conventional MPC that integrates multiple converters into a single unit, the proposed MPC can configure an IH inverter with only a few additional elements. Hence, the proposed MPC achieves the simplified EV power system in comparison with the conventional one [Fig.1(a)].

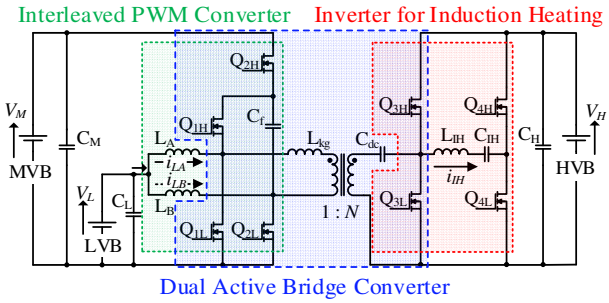

Fig. 3. The proposed MPC.

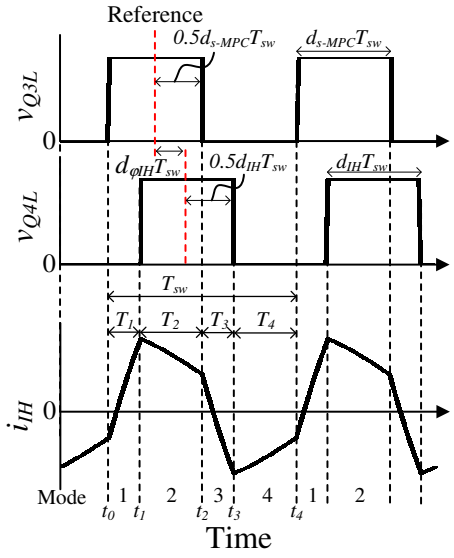

Fig. 4. Key operational waveforms of the IH inverter.

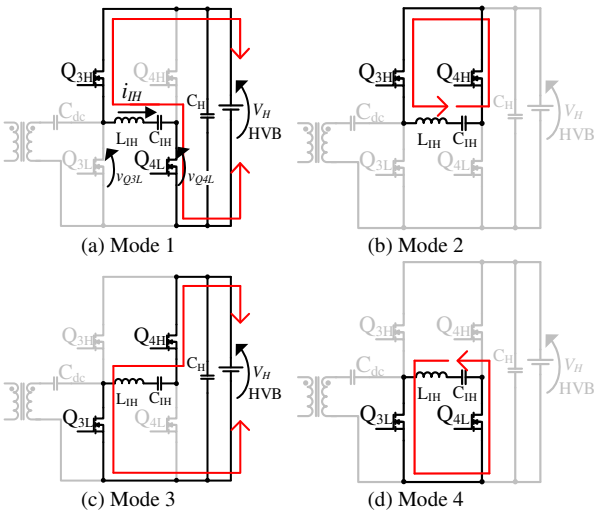

Fig. 5. Current flows of the IH inverter: (a) Mode 1, (b) Mode 2, (c) Mode 3, (d) Mode 4.

B. Control Scheme

PWM and PS controls are applied for the power conversion among batteries. The voltage conversion ratio between the LVB and MVB is regulated with PWM control in the interleaved PWM converter. The power of the HVB, P_H, is regulated with PS control in the DAB converter. On the other hand, one leg of the IH inverter is shared with the DAB converter that operates at a fixed switching frequency. Thus, the IH power, P_{IH}, is regulated with PS control, not with pulse frequency modulation (PFM) control that is employed in ordinary IH inverters [20]–[21].

III. Operational Analysis

There are multiple power flow scenarios depending on the power balance among three battery ports and IH inverter. This paper focuses only on the case that the HVB charges the LVB and MVB. The operational analysis of the low-voltage side is omitted because its operation principle is identical to that of the conventional MPC. Dead-time periods are ignored to simplify the analysis, and all circuit elements are assumed ideal.

A. Operational Principle of IH inverter

Theoretical operational waveforms and current flows of the IH inverter are shown in Figs. 4 and 5, respectively. A single switching cycle is divided into four modes. The duty cycles of Q_{1L}, Q_{2L}, Q_{3L}, and Q_{4L} are defined as d_{MPC}, $d_{p\text{-}MPC}$, $d_{s\text{-}MPC}$ and d_{IH}, respectively, and the PS angle between Q_{3L}–Q_{3H} and Q_{4L}–Q_{4H} is defined as φ_{IH}. Mode length, T_1–T_4, can be expressed as.

$$\begin{cases} T_1 = t_1 - t_0 = \left(\dfrac{d_{s-MPC} - d_{IH}}{2} + d_{\varphi IH}\right) T_{sw} \\ T_2 = t_2 - t_1 = \left(\dfrac{d_{s-MPC} + d_{IH}}{2} - d_{\varphi IH}\right) T_{sw} \\ T_3 = t_3 - t_2 = \left(\dfrac{-d_{s-MPC} + d_{IH}}{2} + d_{\varphi IH}\right) T_{sw} \\ T_4 = t_4 - t_3 = \left(1 - \dfrac{d_{s-MPC} + d_{IH}}{2} - d_{\varphi IH}\right) T_{sw}. \end{cases} \quad (1)$$

where $d_{\varphi IH}$ is the phase-shift duty cycle (= φ_{IH}/360˚), and T_{SW} is the switching period. These duty cycles must satisfy the following conditions to achieve the automatic current balancing between i_{LA} and i_{LB} [1]:

$$\begin{cases} d_{p-MPC} = 0.5 \\ d_{s-MPC} = d_{IH} = d_{MPC} \end{cases} \quad (d_{MPC} < 0.5) \quad (2)$$

$$\begin{cases} d_{p-MPC} = d_{MPC} \\ d_{s-MPC} = d_{IH} = 0.5. \end{cases} \quad (d_{MPC} \geq 0.5) \quad (3)$$

The IH inverter can be equivalently expressed as a typical RLC series circuit. Hence, the current of L_{IH}, i_{IH}, can be calculated from the electric charge of the LC tank, q, and the voltage of C_{IH}, v_C. ω_0, α, β, and θ are defined to simplify the analysis as follows:

$$\begin{cases} \omega_0 = \sqrt{\dfrac{1}{L_{IH}C_{IH}}} \\ \alpha = \dfrac{R_{eq}}{2L_{IH}} \\ \beta = \sqrt{\omega_0^2 - \alpha^2} \\ \theta = tan^{-1}\left(\dfrac{\beta}{\alpha}\right). \end{cases} \quad (4)$$

Mode 1 (t_0–t_1) [Fig. 5(a)]: Before t_0, the current flows through the body diodes of Q_{3H} and Q_{4L}. Q_{3H} turns on, achieving zero voltage switching (ZVS). Since V_H is applied to the LC tank, i_{IH} increases, and the polarity of i_{IH} changes.

First, the initial current of L_{IH} and the initial voltage of C_{IH} are defined as I_0 and V_{C0}, respectively. q is expressed as

$$q(t) = C_{IH}V_H + \frac{1}{\beta}e^{-\alpha t}\{I_0 \sin(\beta t) + \omega_0 C_{IH}(V_{C0} - V_H)\sin(\beta t + \theta)\}. \quad (5)$$

By differentiating (5), i_{IH} can be yielded as

$$i_{IH}(t) = -\frac{\omega_0}{\beta}e^{-\alpha t}\{I_0 \sin(\beta t - \theta) + \omega_0 C_{IH}(V_{C0} - V_H)\sin(\beta t)\}. \quad (6)$$

The voltage of C_{IH}, v_C, is calculated from (5), as

$$v_C(t) = q(t)/C_{IH}. \quad (7)$$

According to (6) and (7), The current and voltage at the end of Mode 1, I_1 and V_{C1}, are derived as follows:

$$I_1 = i_{IH}(t_1). \quad (8)$$

$$V_{C1} = q(t_1)/C_{IH}. \quad (9)$$

Mode2 (t_1–t_2) [Fig. 5(b)]: When Q_{4L} turns off, the current shifts to the body diode of Q_{4H}, achieving ZVS turn-on. The LC tank is short-circuited by Q_{3H} and Q_{4H}.

From I_1 and the initial voltage of C_{IH}, V_{C1}, q is obtained as

$$q(t - t_1) = \frac{1}{\beta}e^{-\alpha(t-t_1)}[I_1 \sin\{\beta(t - t_1)\} + \omega_0 C_{IH}V_{C1}\sin\{\beta(t - t_1) + \theta\}]. \quad (10)$$

Similar to Mode 1, i_{IH} and v_C are obtained as follows:

$$i_{IH}(t - t_1) = -\frac{\omega_0}{\beta}e^{-\alpha(t-t_1)}[I_1 \sin\{\beta(t - t_1) - \theta\} + \omega_0 C_{IH}V_{C1}\sin\{\beta(t - t_1)\}]. \quad (11)$$

$$v_C(t-t_1) = q(t-t_1)/C_{IH} \tag{12}$$

The current and voltage at the end of Mode 2, I_2 and V_{C2}, are derived as

$$I_2 = i_{IH}(t_2 - t_1). \tag{13}$$

$$V_{C2} = q(t_2 - t_1)/C_{IH}. \tag{14}$$

Mode 3 (t_2–t_3) [Fig. 5(c)]: At t_2, Q_{3H} turns off, and the current flows through the body diodes of Q_{3L} and Q_{4H}. At the same time, Q_{3L} turns on, achieving ZVS. Because $-V_H$ is applied to the LC tank, i_{IH} decreases and the polarity of i_{IH} is changed.

From I_2 and the initial voltage of C_{IH} as V_{C2}, q is yielded as

$$\begin{aligned} q(t-t_2) = -C_{IH}V_H + \frac{1}{\beta}e^{-\alpha(t-t_2)}[I_2 \sin\{\beta(t-t_2)\} \\ +\omega_0 C_{IH}(V_{C2}+V_H)\sin\{\beta(t-t_2)+\theta\}]. \end{aligned} \tag{15}$$

Same as Mode 1, i_{IH} and v_C are obtained as follows:

$$\begin{aligned} i_{IH}(t-t_2) = -\frac{\omega_0}{\beta}e^{-\alpha(t-t_2)}[I_2 \sin\{\beta(t-t_2)-\theta\} \\ +\omega_0 C_{IH}(V_{C2}+V_H)\sin\{\beta(t-t_2)\}]. \end{aligned} \tag{16}$$

$$v_C(t-t_2) = q(t-t_2)/C_{IH}. \tag{17}$$

The current and voltage at the end of Mode 3, I_3 and V_{C3}, are derived as (18) and (19).

$$I_3 = i_{IH}(t_3 - t_2). \tag{18}$$

$$V_{C3} = q(t_3 - t_2)/C_{IH}. \tag{19}$$

Mode 4 (t_3–t_4) [Fig. 5(d)]: At t_3, Q_{4H} turns off, and the current shifts to the body diode of Q_{4L}, achieving ZVS turn-on. The LC tank is short-circuited by Q_{3L} and Q_{4L}. From I_4 and the initial voltage of C_{IH} as V_{C4}, q is

$$\begin{aligned} q(t-t_3) = \frac{1}{\beta}e^{-\alpha(t-t_3)}[I_3 \sin\{\beta(t-t_3)\} \\ +\omega_0 C_{IH}V_{C3}\sin\{\beta(t-t_3)+\theta\}]. \end{aligned} \tag{20}$$

With reference to Mode 1, i_{IH} and v_C are obtained as follows:

$$\begin{aligned} i_{IH}(t-t_3) = -\frac{\omega_0}{\beta}e^{-\alpha(t-t_3)}[I_3 \sin\{\beta(t-t_3)-\theta\} \\ +\omega_0 C_{IH}V_{C3}\sin\{\beta(t-t_3)\}]. \end{aligned} \tag{21}$$

$$v_C(t-t_3) = q(t-t_3)/C_{IH}. \tag{22}$$

The current and voltage at the end of Mode 4, I_4 and V_{C4}, are derived as (23) and (24).

$$I_4 = i_{IH}(t_4 - t_3) = I_0. \tag{23}$$

$$V_{C4} = q(t_4 - t_3)/C_{IH} = V_{C0}. \tag{24}$$

In conclusion, I_0 and V_0 can be calculated from (23) and (24), and the current of L_{IH} and the voltage of C_{IH} in each mode are determined.

B. Theoretical Output Characteristics of IH Inverter

The output power of the IH inverter, P_{IH}, is

$$P_{IH} = R_{eq}I_{rms}^2. \tag{25}$$

where R_{eq} is the equivalent resistance of the workpiece, and I_{rms} is the RMS value of i_{IH}. In general, I_{rms} is given by

$$I_{rms} = \sqrt{\frac{\int_0^{T_{sw}} i_{(t)}^2 dt}{T_{sw}}}. \tag{26}$$

P_{IH} is expressed as

$$\begin{aligned} P_{IH} = \frac{R_{eq}}{T_{sw}}\left(\int_0^{T_1}\{i_{IH}^2(t)\}dt + \int_0^{T_2}\{i_{IH}^2(t)\}dt \right. \\ \left. + \int_0^{T_3}\{i_{IH}^2(t)\}dt + \int_0^{T_4}\{i_{IH}^2(t)\}dt\right). \end{aligned} \tag{27}$$

The theoretical characteristic of I_{rms} as a function of φ_{IH} is shown in Fig. 6. P_{IH} can be regulated arbitrarily by adjusting φ_{IH}, though I_{rms} is slightly influenced by variations in $d_{s\text{-}MPC}$ and d_{IH}, which are manipulated to regulate the voltage conversion ratio between the LVB and MVB.

C. Simultaneous Operation for MPC and IH Inverter

The proposed MPC can regulate P_H and P_{IH} simultaneously by using two control freedoms, φ_{MPC}, and φ_{IH}. φ_{MPC} is the PS angle between Q_{1L}–Q_{1H} and Q_{3L}–Q_{3H}.

Refer to [1], P_H is given by

$$P_H = \frac{V_M V_H d_{\varphi MPC}\{2d_{MPC}(1-d_{MPC}) + d_{\varphi MPC}\}}{2Nf_{sw}L_{kg}}, \tag{28}$$

where N is the transformer turns ratio, L_{kg} is the leakage inductance of the low-voltage side, and $d_{\varphi MPC}$ is the phase-shift duty cycle (= φ_{MPC}/360˚). (27) and (28) suggest P_H and P_{IH} can be independently regulated by φ_{MPC} and φ_{IH}, respectively, with no interaction because these equations contain only one phase-shift duty cycle.

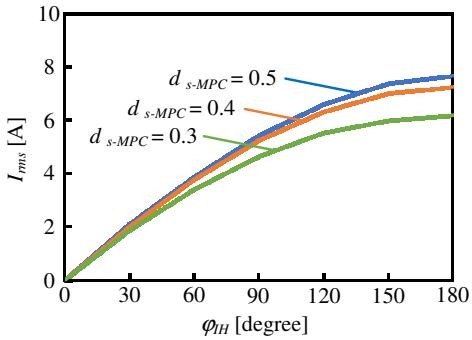

Fig. 6. Theoretical characteristics of I_{rms} as a function of φ_{IH} with different duty cycle $d_{s\text{-}MPC}$.

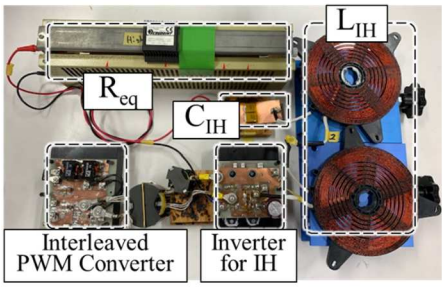

Fig. 7. 1 kW-prototype of proposed MPC.

TABLE I. KEY ELEMENTS OF THE PROTOTYPE

Components	***Parameters***
C_L	Ceramic Capacitor, 100 µF
C_M	Ceramic Capacitor, 150 µF
C_H	Aluminum Electrolytic Capacitor, 180 µF
C_f	Ceramic Capacitor, 200 µF
C_{dc}	Ceramic Capacitor, 17.6 µF
L_A, L_B	15 µH, R_{dc} = 2.4 mΩ
Q_{1H}	IRFP4110PbF, V_{DS} = 100 V, R_{on} = 4.5 mΩ
Q_{1L}, Q_{2L}, Q_{2H}	IRFP7530PbF, V_{DS} = 60 V, R_{on} = 2 mΩ
Q_{3L}, Q_{3H}, Q_{4L}, Q_{4H}	C3M0120090D, V_{DS} = 900 V, R_{on} = 120 mΩ
C_{IH}	Film Capacitor, 348.5 nF
L_{IH}	133 µH, R_{dc} = 377 mΩ
R_{eq}	15.1 Ω
Gate Driver	ADuM3223ARZ

IV. Experimental Results

A 1-kW prototype of the proposed MPC was built, as shown in Fig. 7. Component values are listed in Table I. A 15 Ω resister was connected in series with the LC tank to simulate the equivalent resistance of the workpiece, R_{eq}. The prototype

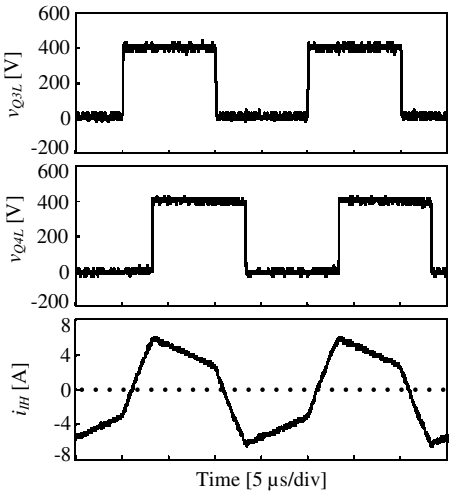

Fig. 8. Experimental waveforms of IH inverter with φ_{IH} = 60° and $d_{s\text{-}MPC}$ = 0.5.

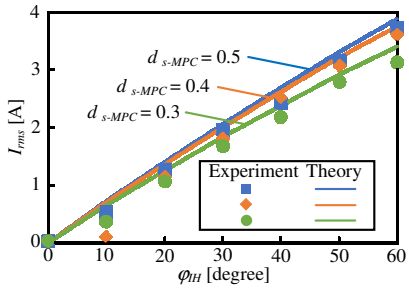

Fig. 9. Output current I_{rms} as a function of φ_{IH} with different duty cycle $d_{s\text{-}MPC}$.

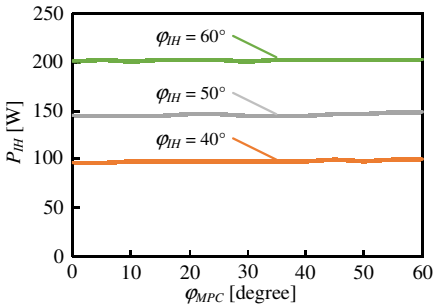

Fig. 10. Output power P_{IH} as a function of phase-shift angle φ_{MPC} with different phase-shift angle φ_{IH}.

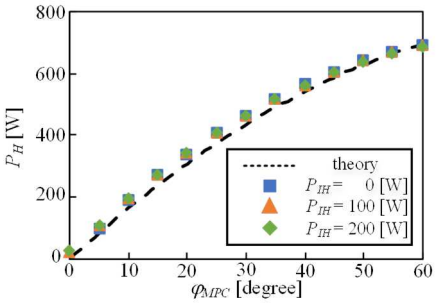

Fig. 11. Output power P_H as a function of phase-shift angle φ_{MPC} with different output power P_{IH}.

operated with V_L = 12 V, V_M = 48 V, and V_H = 400 V at the switching frequency of 50 kHz.

A. Waveforms and Output Characteristics of IH Inverter

Experimental waveforms of the IH inverter with φ_{IH} = 60° and $d_{s\text{-}MPC}$ = 0.5 are shown in Fig. 8. The experimental results matched satisfactorily with the theoretical one (see Fig. 5), verifying the operation of the prototype.

I_{rms} as a function of φ_{IH} with different duty cycles $d_{s\text{-}MPC}$ are shown in Fig. 9. I_{rms} could be regulated by φ_{IH}. Meanwhile, the measured value currents were slightly lower than the theoretical ones probably due to neglected parameters, such as dead-time periods and parasitic components.

B. Simultaneous Operation for MPC and IH Inverter

P_{IH} as a function of φ_{MPC} with $d_{s\text{-}MPC}$ = 0.5 are shown in Fig. 10. The result revealed that P_{IH} was determined without depending on φ_{MPC}. On the other hand, P_H as a function of φ_{MPC} with $d_{s\text{-}MPC}$ = 0.5 is shown in Fig. 11. The results demonstrated that P_H matched well with theoretical output characteristic. In conclusion, these results indicated that P_H and P_{IH} have no interaction and can be regulated individually.

V. Conclusion

This paper has proposed the novel MPC integrating the IH inverter for EV power systems. The MPT and IH inverter are integrated into a single unit with sharing switches, achieving simplified system and reduced cost. The detailed operational analysis of the IH inverter was performed to derive the theoretical output characteristics.

The experimental verification using the 1-kW prototype demonstrated the proposed MPC could transfer power among batteries and regulate the output power of the IH inverter simultaneously.

References

[1] M. Sato, Y. Tada, Y. Sato, and M. Uno, "Interleaved Multi-Port Converter with High Voltage-Conversion Ratio and Automatic Current Balancing Capability for Electric Vehicle," I. E. E. Japan, 4-119, Mar.2019

[2] J. Zhang, H. Wu, X. Qin, and Y. Xing, "PWM Plus Secondary-Side Phase-Shift Controlled Soft-Switching Full-Bridge Three-Port Converter for Renewable Power Systems," IEEE Trans. Industrial Electron., vol. 62, no. 11, pp. 7061-7072, Nov.2015.

[3] L. Solero, A. Lidozzi, and J. A. Pomilio, "Design of Multiple-Input Power Converter for Hybrid Vehicles," IEEE Trans. Power Electron., vol. 20, no 5, pp. 1007-1016, Sep.2005.

[4] T. Bhattacharya, V. Shriganesh Giri, K. Mathew, and L. Umanand, "Multiphase Bidirectional Flyback Converter Topology for Hybrid Electric Vehicles," IEEE Trans. Industrial Electron., vol 56, no. 1, pp. 78-84, Jan.2009.

[5] H. Krishnaswami, and N. Mohan, "Three-Port Series-Resonant DC–DC Converter to Interface Renewable Energy Sources With Bidirectional Load and Energy Storage Ports," IEEE Trans. Power Electron., vol. 24, no. 10, pp. 2289-2297, Oct.2009.

[6] H. Wu, P. Xu, H. Hu, Z. Zhou, and Y. Xing, "Multiport Converters Based on Integration of Full-Bridge and Bidirectional DC–DC Topologies for Renewable Generation Systems," IEEE Trans. Industrial Electron., vol. 61, no. 2, pp. 856-869, Feb.2014.

[7] X. Sun, Y. Shen, W. Li, and H. Wu, "A PWM and PFM Hybrid Modulated Three-Port Converter for a Standalone PVBattery Power System," IEEE Journal. Power Electron., vol. 3, no. 4, pp. 984-1000, Dec.2015.

[8] W. Li, X. Yi Zhao, and X He, "PWM plus phase angle shift (PPAS) control scheme for combined multiport dc/dc converters", IEEE Trans. Power Electron., vol. 27, no. 3, pp. 1479–1489, Mar. 2012.

[9] M. Mira, Z. Zhang, A. Knott, and M. Anderson, "Analysis, design, modeling, and control of an interleaved-boost full-bridge three-port converter for hybrid renewable energy systems", IEEE Trans. Power Electron., vol. 32, no. 2, pp. 1138–1155, Feb. 2017.

[10] Z. Wang, and H Li, "An Integrated Three-Port Bidirectional DC–DC Converter for PV Application on a DC Distribution System", IEEE Trans. Power Electron., vol. 28, no. 10, pp. 4612–4624, Oct. 2013.

[11] Z. Ding, C. Yang, Z. Zhang, C. Wang, and S. Xie, "A Novel Soft-Switching Multiport Bidirectional DC–DC Converter for Hybrid Energy Storage System", IEEE Trans. Power Electron., vol. 29, no. 4, pp. 1595–1609, Apr. 2014.

[12] H. Sarnago, O. Lucía, and J. M. Burdio, "A Versatile Resonant Tank Identification Methodology for Induction Heating Systems," IEEE Trans. Power Electron., vol. 33, no. 3, pp. 1897-1901, Mar.2018.

[13] H. P. Park, and J. H. Jung, "Load-adaptive modulation of a series-resonant inverter for all-metal induction heating applications," IEEE Trans. Industrial Electron., vol. 65, no 9, pp. 6983-6993, Jan.2018.

[14] P. Viriya, N. Yongyuth, I. Miki, and K. Matsuse. "Analysis of Circuit Operation under ZVS and NON-ZVS Conditions in Phase-Shift Inverter for Induction Heating," IEEJ Trans. Industrial App., vol. 126, no. 5, pp. 560-567, 2006.

[15] N. A. Ahmed, and M. Nakaoka, " Boost-half-bridge edge resonant soft switching PWM high-frequency inverter for consumer induction heating appliances," IEE Proc. Electric power App., vol. 153, no. 6, pp. 932-938, Nov.2006.

[16] P. Hothongkham, and V. kinnares, "Analysis and Modelling of an Ozone Generator Using a Phase-Shift PWM Full Bridge Inverter," 2008 IEEE International conference on Robotics.

[17] M. Uno, M. Inoue, Y. Sato, and H. Nagata, "Bidirectional Interleaved PWM Converter with High Voltage-Conversion Ratio and Automatic Current Balancing Capability for Single-Cell Battery Power System in Small Scientific Satellites," energies, vol. 11, no. 10, Oct.2018.

[18] K. Xiangli, S. Li, and K. M. Smedley "Decoupled PWM Plus Phase-Shift Control for a Dual-Half-Bridge Bidirectional DC-DC Converter," IEEE Trans. Power Electron., vol. 33, no. 8, pp. 7203-7213, Oct.2017.

[19] O. Lucía, P. Maussion, E. J. Dede, and J. M. Burdío, "Induction Heating Technology and its Applications Past Developments, Current Technology, and Future Challenges," IEEE Trans. Industrial Electron., vol. 61, no. 5, pp. 2509-2520, May.2014.

[20] B. Saha, and R. Y. Kim, "High Power Density Series Resonant Inverter Using an Auxiliary Switched Capacitor Cell for Induction Heating Applications," IEEE Trans. Power Electron., vol 29, no 4, pp. 1909-1918, Jan.2014.

[21] Y. S. Kwon, S. B. Yoo, and D. S. Hyun, "Half-Bridge Series Resonant Inverter for Induction Heating Applications with load-adaptive PFM control strategy." IEEE Appl. Power Electron., pp. 57-581, 1999.

[22] T. Ariga, "Air Conditioner Having Positive Temperature Coefficient Heater," United State Patent, US 9,182,134 B2, Nov.2015.

[23] M. H. Park, and S. C. Kim, "Heating Performance Enhancement of High Capacity PTC Heater with Modified Louver Fin for Electric Vehicles," Energies, vol. 12, no. 15, pp. 2900, July.2019.

[24] H.S. Lee, J. P. Won, C. W. Cho, Y. C. Kim, and M. Y. Lee, "Heating performance characteristics of stack coolant source heat pump using R744 for fuel cell electric vehicles," Journal of Mechanical Science and Technology, vol. 26, no. 7, pp. 2065-2071, July.2012.

[25] H. Bayram, G. Sevilgen, and M. Kılıç, "Advances on Heat Pump Applications for Electric Vehicles," Advances in Automotive Engineering, Vol. 1, No. 1, pp. 79-104, Mar.2018.

[26] O. Takagi, and S. Kinouchi, "Fixing Device Using Induction Heating Technology," Journal of the Imaging Society of Japan, vol. 43, no. 6, pp.459-465, July.2006.

[27] K. Kusaka, and J. Itoh, "Experimental Verification of Non-resonant Wireless Power Transfer System Based on an Operation Principle of Dual Active Bridge Converter," IEE Japan 2015(112-118),17-22, July.2015.